J|A|C|S ARTICLES

Published on Web 07/27/2010

Selective Synthesis of Subnanometer Diameter Semiconducting Single-Walled Carbon Nanotubes

Codruta Zoican Loebick,[†] Ramakrishna Podila,[‡] Jason Reppert,[‡] Joel Chudow,[†] Fang Ren,[†] Gary L. Haller,[†] Apparao M. Rao,[‡] and Lisa D. Pfefferle*,[†]

Department of Chemical Engineering, Yale University, New Haven, Connecticut 06513, and Department of Physics and Astronomy and Center for Optical Material Science and Engineering Technologies, Clemson University, Clemson, South Carolina 29634

Received March 9, 2010; E-mail: lisa.pfefferle@yale.edu

Abstract: Subnanometer single-walled carbon nanotubes (sub-nm SWNTs) were synthesized at different temperatures (600, 700, and 800 °C) using CoMn bimetallic catalysts supported on MCM-41 silica templates. The state of the catalyst was investigated using X-ray absorption, and the (*n*,*m*) indices of the sub-nm SWNTs were determined from Raman spectroscopy and photoluminescence measurements. We find that the size of the metallic particles that seed the growth of sub-nm SWNTs (diameter ~0.5−1.0 nm) is highly sensitive to the reaction temperature. Low reaction temperature (600 °C) favors the growth of semiconducting tubes whose diameters range from 0.5 to 0.7 nm. These results were also confirmed by electrical transport measurements. Interestingly, dominant intermediate frequency modes on the same intensity scale as the Raman breathing modes were observed. An unusual "S-like" dispersion of the G-band was present in the Raman spectra of sub-nm SWNTs with diameters <0.7 nm.

1. Introduction

SWNTs are one-dimensional systems with exceptional chemical and electronic properties and a vast number of emerging applications.[1−3] To date, much research effort has been dedicated to producing SWNT materials with a narrow diameter distribution and specific (*n*,*m*) indices. These indices are related to the chiral vector $C_h = na_1 + ma_2$, where (a_1,a_2) are the unit vectors of graphene.[4−7] Synthesis of nanotubes with specific (*n*,*m*) indices is important for the advancement of SWNTs in electronic applications. The general mechanism by which SWNTs are produced consists of exposing catalytic transition metal particles (especially Fe, Co, and Ni) to a carbon feedstock (CO, ethane, acetylene, etc.) at high temperatures (between 500 and 1000 °C) and varying pressures. When the catalyst particles become saturated with carbon, the growth of SWNTs is initiated by the formation of a stable carbon cap at the surface of the particle, followed by addition of carbon atoms at the growing end of the cap to form a nanotube. The diameter and symmetry of the carbon cap should closely match those of the metal particle.[8,9]

Previously, Ding et al.[10] showed that the interaction between the end atoms of a growing SWNT and the catalyst metal atoms has a high bond energy, and the enthalpy of SWNT formation is substantially reduced when the number of carbon−metal bonds is maximized. A key factor in diameter-selective synthesis of SWNTs is therefore the size of the catalyst particles.[9,10] We have previously shown that diameter-selective growth of SWNTs can be achieved using MCM-41 mesoporous silica templates isomorphously substituted with Co.[11,12] Here, we demonstrate an improved synthesis method in which a second transitional metal (Mn) is added to the aforementioned Co-MCM-41 monometallic system. The second metal component does not form metallic particles during synthesis due to its high stability against reduction. Instead, Mn ions highly dispersed in the silica substrate act as anchoring sites for small Co particles, preventing them from sintering into large, inert particles.[13] Similar results were obtained with a CoCr-MCM-41 bimetallic system.[14,15] A combined photoluminescence and Raman study showed that the CoMn-MCM-41 catalyst with a

[†] Yale University.
[‡] Clemson University.

(1) Saito, R.; Dresselahus, G.; Dresselahus, M. S. *Phys. Rev. B* **2000**, *61*, 2981.
(2) Zheng, B.; Lu, C.; Gu, G.; Makarovski, A.; Finkelstein, G.; Liu, J. *Nano Lett.* **2002**, *2*, 895.
(3) Baughman, R. H.; Zakhidov, A. A.; de Heer, W. A. *Science* **2002**, *297*, 787.
(4) Herrera, J. E.; Balzano, L.; Borgona, A.; Alvarez, W. E.; Resasco, D. E. *J. Catal.* **2001**, *204*, 129.
(5) Herrera, J. E.; Resasco, D. E. *J. Phys. Chem. B* **2003**, *107*, 3738.
(6) Miyauchi, Y.; Chiashi, S.; Marukami, Y.; Hayashida, Y.; Maruyama, S. *Chem. Phys. Lett.* **2004**, *387*, 198.
(7) Ago, H.; Imamura, S.; Okazaki, T.; Saito, T.; Yumura, M.; Tsuji, M. *J. Phys. Chem. B* **2005**, *109*, 10035.
(8) Jorio, A.; Dresselhaus, M. S.; Dresselhaus, G. *Carbon Nanotubes*, Topics in Applied Physics*111*; Springer: Berlin, 2008.
(9) Ding, F.; Bolton, K.; Rosen, A. *J. Phys. Chem. B* **2004**, *108*, 17369.
(10) Ding, F.; Rosen, A.; Bolton, K. *Chem. Phys. Lett.* **2004**, *393*, 309.
(11) Ciuparu, D.; Chen, Y.; Lim, S.; Haller, G. L.; Pfefferle, L. *J. Phys. Chem. B* **2004**, *108*, 503.
(12) Lim, S.; Li, N.; Fang, F.; Pinault, M.; Zoican, C.; Wang, C.; Fadel, T.; Pfefferle, L. D.; Haller, G. L. *J. Phys. Chem. C* **2008**, *112*, 12442.
(13) Zoican Loebick, C.; Derrouiche, S.; Marinkovic, N.; Wang, C.; Hennrich, F.; Kappes, M. M.; Haller, G. L.; Pfefferle, L. D. *J. Phys. Chem. C* **2009**, *113*, 21611.
(14) Zoican Loebick, C.; Derrouiche, S.; Fang, F.; Li, N.; Haller, G. L.; Pfefferle, L. D. *Appl. Catal., A* **2009**, *368*, 40.

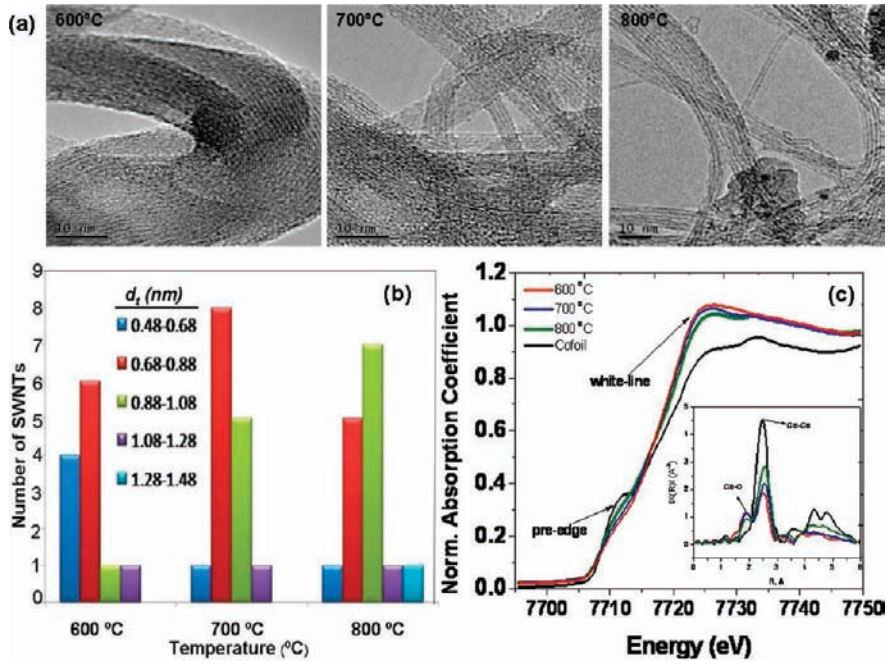

Figure 1. (a) TEM of as-prepared sub-nm SWNTs synthesized at 600, 700, and 800 °C using CoMn-MCM-41 bimetallic catalyst. The scale bar shown in each micrograph is 10 nm. (b) Diameter distribution of sub-nm SWNTs shown in (a) obtained from a combined PL and Raman study. (c) Co K-edge EXAFS spectra of the catalyst after SWNT synthesis at the three temperatures. The inset shows a Fourier transform of (c).

molar ratio of 1:3 favors the growth of semiconducting, subnanometer diameter (sub-nm) SWNTs. Importantly, with decreasing synthesis temperature, a gradual increase in the proportion of semiconducting sub-nm SWNTs formed is observed. In addition, strong intermediate frequency modes (IFMs) are observed in the Raman spectra excited with $\lambda_{\text{excitation}} = 785$, 855, and 1064 nm.

2. Results and Discussion

A CoMn-MCM-41 catalyst with 3% metal loading (Co:Mn in a molar ratio of 1:3) was synthesized by isomorphous substitution of metal in the silica framework. A 16-carbon-atom alkyl chain length was used to template the MCM-41, yielding an average pore diameter of about 3 nm, as determined by nitrogen physisorption measurements. Details of the experimental procedure are given elsewhere.[13,16] Briefly, sub-nm SWNTs were prepared using the CoMn-MCM-41 catalyst (~200 mg) from a thermal disproportionation of CO (1000 sccm) at 600, 700, and 800 °C in a quartz tube (diameter ~18 mm) reactor. The metal ions in the CoMn-MCM-41 catalyst were partially reduced (flowing hydrogen at 1000 sccm, 700 °C, 1 atm) prior to CO disproportionation.[13] The products were extensively characterized using transmission electron microscopy (TEM), extended X-ray absorption fine structure (EXAFS), photoluminescence (PL), and Raman spectroscopy.

Representative TEM images of sub-nm SWNT bundles synthesized at the three temperatures (600, 700, and 800 °C) are shown in Figure 1a. These samples exhibit a narrow diameter distribution (0.5−0.9 nm), as evidenced in Figure 1b. Clearly, a lower synthesis temperature favors the growth of smaller diameter sub-nm SWNT (0.5−0.7 nm).

As shown by previous research,[11−15] in the MCM-41 system, most of the cobalt particles formed during synthesis are embedded on the MCM-41 pore wall. Very few of these particles are visible on the catalyst surface, such that they are not readily available for TEM or SEM measurements.

EXAFS spectroscopy offers a convenient way for determining the mean size of catalyst particles since it is a volume-average technique (Figure 1c).[13] The first-shell Co−Co coordination number determined from the EXAFS data analysis is shown in Table S1 in the Supporting Information. The Co foil reference spectrum exhibits a strong pre-edge feature which is assigned to dipole-forbidden transitions in the metallic Co. This feature is also present in the corresponding spectra of as-reacted catalysts, confirming that Co is predominantly in a zerovalent state, consistent with the formation of metallic Co particles during sub-nm SWNTs synthesis. Another region of interest is the white-line feature assigned to unfilled d states at the Fermi level. The low intensity of this feature further confirms the presence of metallic Co in the as-reacted catalyst.[17] The inset in Figure 1c is the Fourier transform of the EXAFS spectrum, which gives the radial distribution function. For all samples, the most intense peak is ascribed to the second-shell Co−Co bond (2.4 Å),while a less intense feature at 1.9 Å is ascribed to the first-shell Co−O bond.[17] We find that the average size of the Co particle increases with the reaction temperature from 0.8 nm at 600 °C to 0.9 nm at 700 °C and 1.25 nm at 800 °C. This is an expected result, as higher temperatures accelerate the rate of metal agglomeration,causing the particles to increase in size. It is important to note that a certain degree of uncertainty must be added to the particle size calculations from EXAFS data. Since this is a volume-average technique, some of the larger particles formed due to sintering of un-incorporated Co can affect the end result of the fitting. These larger particles do

(15) Zoican Loebick, C.; Abanulo, D.; Majewska, M.; Haller, G. L.; Pfefferle, L. D. *Appl. Catal., A* **2010**, *107*, 11048.
(16) Chen, Y.; Ciuparu, D.; Lim, S.; Yang, Y.; Haller, G.; Pfefferle, L. *J. Catal.* **2004**, *225*, 453.
(17) Ciuparu, D.; Chen, Y.; Lim, S.; Yang, Y.; Haller, G.; Pfefferle, L. *J. Phys. Chem. B* **2004**, *108*, 15565.

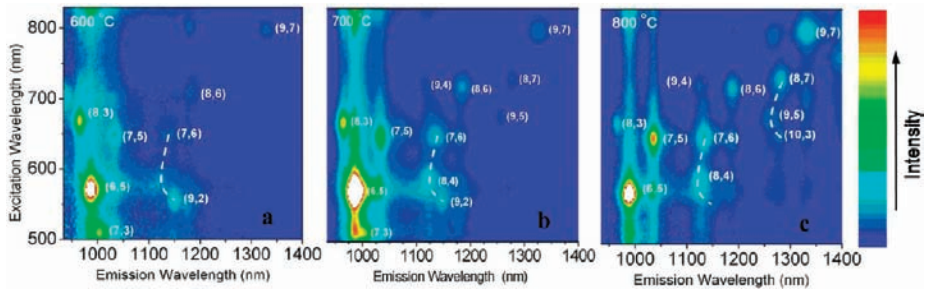

Figure 2. PL contour mapping of the sub-nm SWNTs shown in Figure 1a. The (*n*,*m*) indices were obtained using a Kataura plot. The family lines for $2n + m = 20$ and 23 are shown (dashed white lines). Other families are only partially observed ($2n + m = 17$, 19, and 22).

not contribute to SWNT formation; therefore, the average size of the particles directly responsible for the nanotube growth can be somewhat smaller than the size calculated from the EXAFS data. The decrease in particle size with the decrease of reaction temperature is, however, important and cannot be attributed to error. This fact is also evident from the shift in the SWNT diameter (see Raman and PL data). Mn cannot initiate the growth of SWNT by itself because it does not reduce to metallic state in the conditions employed in our experiments. Mn ions dispersed in the framework act as anchoring sites for small, narrowly distributed Co particles, as shown in our previous research.[13]

It is possible that, for a given particle size, the resulting SWNTs can have the same diameter but different (*n*,*m*) indices. For example, Miyuachi and co-workers[18] have reported that the number of possible cap structures for small-diameter tubes (<0.8 nm diameter) is few but increases exponentially for larger diameter tubes. For example, (6,5) and (9,1) SWNTs, which have the same diameter, have a unique possible cap structure, which satisfies the isolated pentagon rule.[18] In their experiment, the yield of the (6,5) tube was predominant as compared to the (9,1) tube, and this observation was attributed to the relatively lower activation (kinetic) energy for the (6,5) tube.

PL has been used extensively for identifying (*n*,*m*) indices of semiconducting SWNTs and their relative abundance.[19,20] The excitonic contributions to the SWNT electronic properties make precise (*n*,*m*) indexing difficult; however, estimates are possible.[20] Figure 2 shows the contour maps of normalized intensities from the PL spectra. Each distinct peak corresponds to an emission from the first band gap (E_{11}) of a semiconducting sub-nm SWNT. (*n*,*m*) indices of the most abundant sub-nm SWNTs are identified in the PL spectra, and their relative abundance (Table 1, Supporting Information Figure S1) was determined from direct measurements of the peak intensities (15% accuracy). Consistent with the Raman analysis discussed below, the dominant semiconducting sub-nm SWNT is the (6,5), with a relative abundance (Figure 2b, Figure S1) of ~40% in all samples and a maximum of ~45% at 700 °C. It should be mentioned that the smallest sub-nm SWNT accessible in our PL experiments is the (7,3) with a diameter of 0.706 nm, although SWNTs of smaller diameter were identified in our samples by TEM and Raman spectroscopy as shown next.

Resonant Raman scattering in SWNT bundles results from the sharp van Hove singularities present in their electronic density of states. Thus, for a given excitation energy used in the experiment, a subset of the SWNT population can be probed.[21−24] In Figures 3−5 and Supporting Information Figure S2a−c, room-temperature Raman spectra for sub-nm SWNTs as-synthesized at 600, 700, and 800 °C are shown. Spectra were collected at seven different laser excitation wavelengths for each sample: $\lambda_{excitation} = 488$, 514, 532, 647, 785, 855, and 1064 nm. Apart from the radial breathing modes (RBMs), the disorder band (D-band), and the tangential stretching modes (G-band), a rich set of intermediate frequency modes (IFMs) are observed in the samples reacted at the lower temperature, which contain mainly sub-nm semiconducting SWNTs (Figure 3b, c). These strong IFMs were also noted in SWNTs grown on a CoCr catalyst at 600 °C,[15] where small-diameter semiconducting SWNTs were observed. Detailed analysis of such IFMs will be pubished separately (R. Podila et al.).

Table 1. (*n*,*m*) Resolved Spectral Intensities from SWNT Samples Synthesized on the CoMn-MCM-41 Catalyst at Different Temperatures

(*n*,*m*)	diameter, nm	CoMn 1:3, 600 °C	CoMn 1:3, 700 °C	CoMn 1:3, 800 °C
(6,5)	0.757	39.7	44.5	38.6
(7,3)	0.706	18.7	16.4	0
(7,5)	0.829	8.5	9.7	20.9
(7,6)	0.895	2.0	3.0	7.5
(8,3)	0.782	20.4	13.4	5.0
(8,4)	0.840	0	4.1	7.0
(8,6)	0.966	1.9	2.3	4.3
(8,7)	1.032	0	1.3	4.5
(9,2)	0.806	6.4	3.0	0
(9,7)	1.103	2.3	1.7	6.1

For SWNT bundles, it is well known that the frequency of the RBM peaks (ω_{RBM}) is inversely related to the SWNT diameter d_t as

$$\omega_{RBM} = \frac{223.5\ \text{cm}^{-1}\ \text{nm}}{d_t} + 12.5\ \text{cm}^{-1} \qquad (1)$$

A clear shift of the RBM position toward higher values (lower tube diameter) is noted as the reaction temperature is decreased. In the sample reacted at 600 °C, tubes with diameters as low as

(18) Miyauchi, Y.; Chiashi, S.; Marukami, Y.; Maruyama, S. *Chem. Phys. Lett.* **2004**, *387*, 198.
(19) Weisman, R.; Bachilo, S. *Nano Lett.* **2003**, *3*, 1235.
(20) Bachilo, S.; Balzano, L.; Herrera, J.; Pompeo, F.; Resasco, D. E.; Weisman, R. *J. Am. Chem. Soc.* **2003**, *125*, 11186.
(21) Rao, A. M.; Richter, E.; Bandow, S.; Chase, B.; Eklund, P. C.; Williams, K. W.; Menon, M.; Subbaswamy, K. R.; Thess, A.; Smalley, R. E.; Dresselhaus, G.; Dresselhaus, M. S. *Science* **1997**, *275*, 187.
(22) Jorio, A.; Santos, A. P.; Ribeiro, H. B.; Fantini, C.; Vieira, J. P. M.; Furtado, C. A.; Jiang, J.; Saito, R.; Balzano, L.; Resasco, D. E.; Pimenta, M. A. *Phys. Rev. B* **2005**, *72*, 075207.
(23) Dresselhaus, M. S.; Dresselhaus, G.; Jorio, A. *J. Phys. Chem. C* **2007**, *111*, 17887.
(24) Jorio, A.; Saito, R.; Hafner, J. H.; Lieber, C. M.; Hunter, M.; McClure, T.; Dresselhaus, G.; Dresselhaus, M. S. *Phys. Rev. Lett.* **2001**, *86*, 1118.

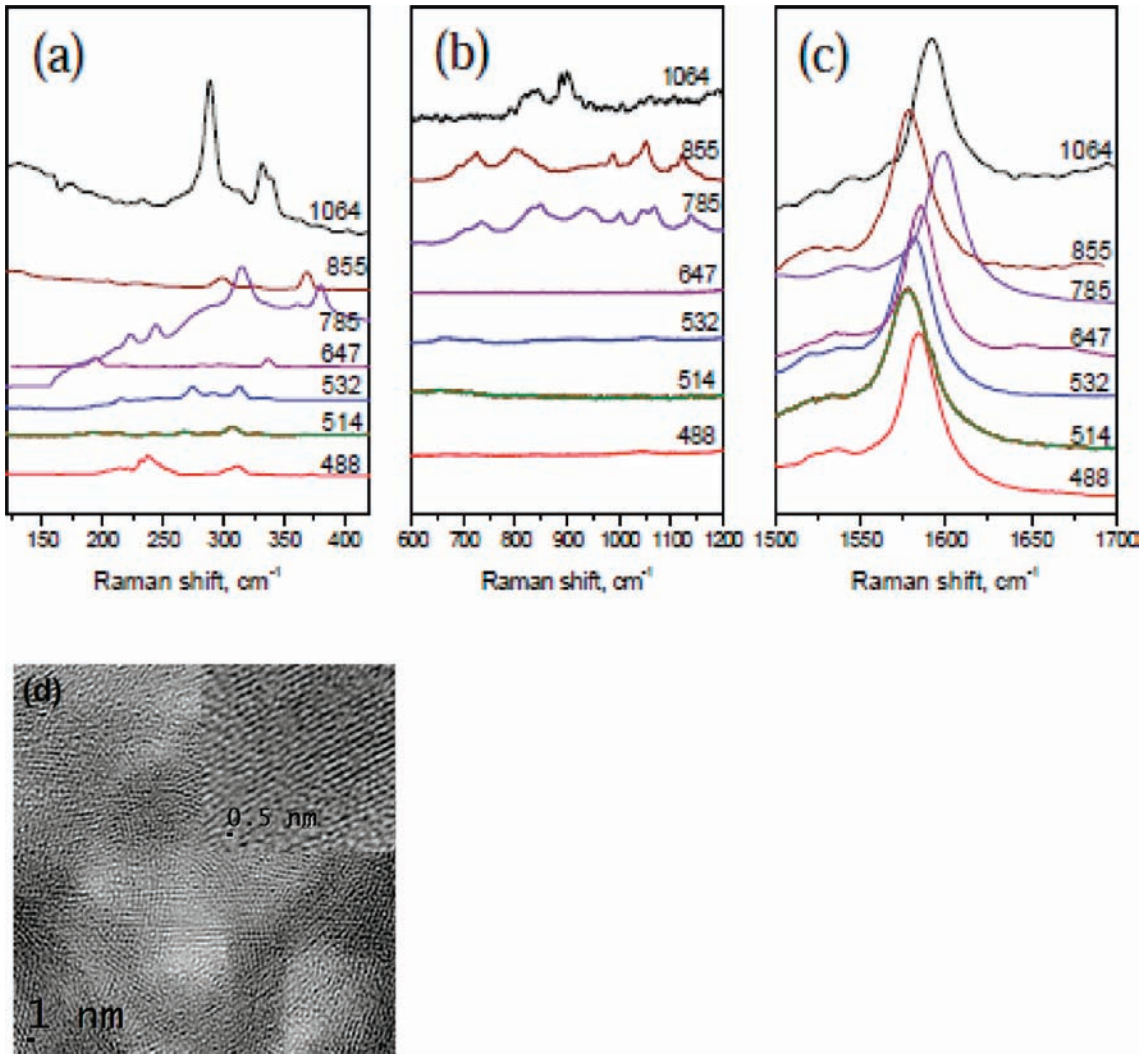

Figure 3. Raman spectra, normalized to the intensity of the G-band, of sub-nm SWNTs prepared at 600 °C: (a) radial breathing modes [(*n*,*m*) indexed spectra can be found in Figure S3a in the Supporting Information], (b) intermediate frequency modes, and (c) "S-like" G-band dispersion. (d) High-resolution TEM image for SWNT bundles synthesized at 600 °C.

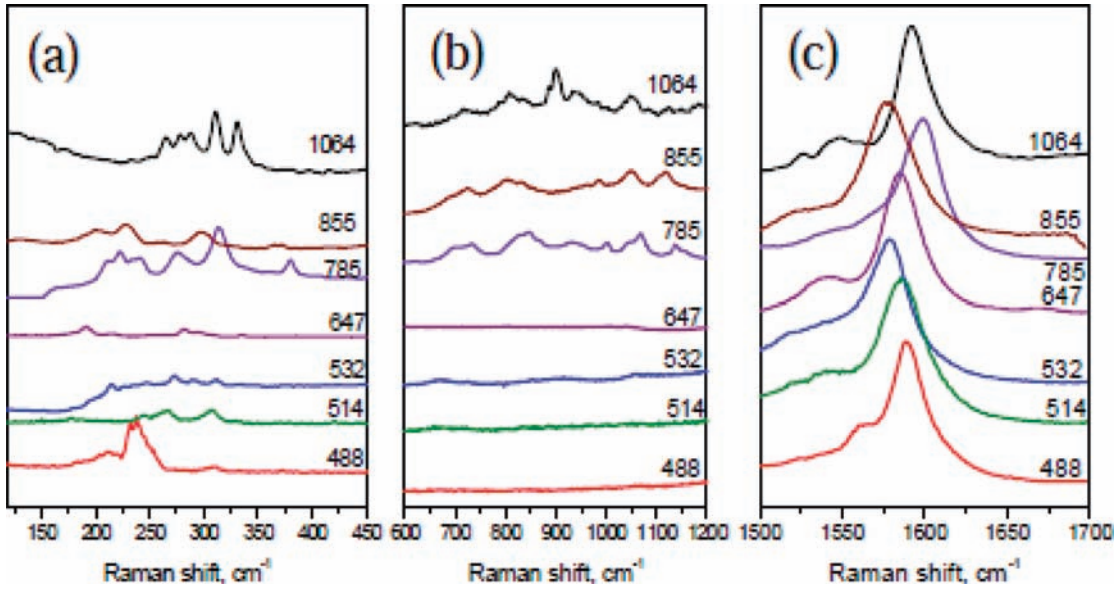

Figure 4. Raman spectra, normalized to the intensity of the G-band, of sub-nm SWNTs prepared at 700 °C: (a) radial breathing modes [(*n*,*m*) indexed spectra can be found in Figure S3b in the Supporting Information], (b) intermediate frequency modes, and (c) G-band dispersion.

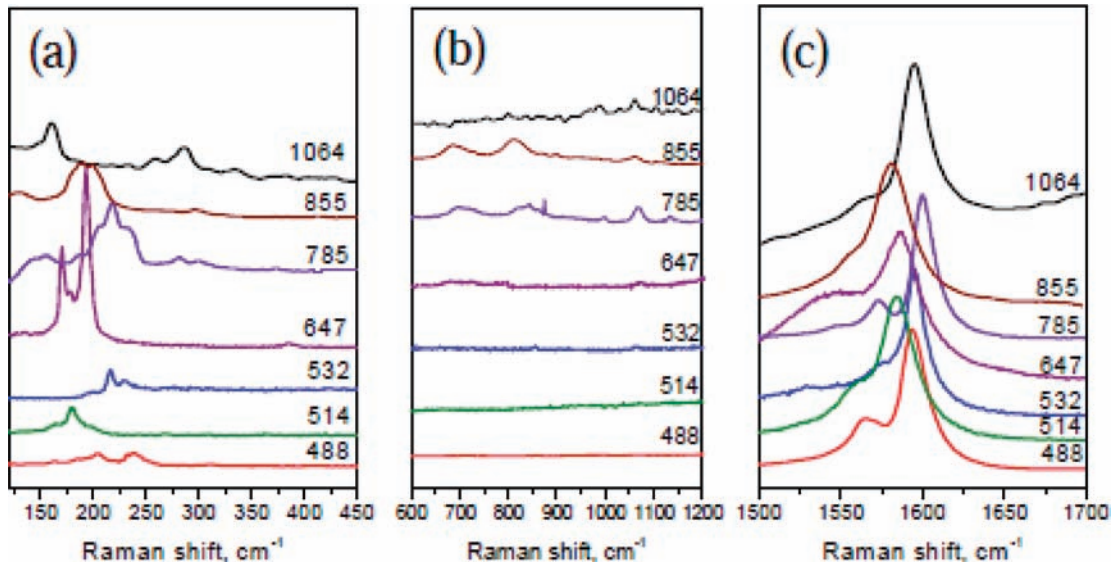

Figure 5. Raman spectra, normalized to the intensity of the G-band, of sub-nm SWNTs prepared at 800 °C: (a) radial breathing modes [(*n*,*m*) indexed spectra can be found in Figure S3c in the Supporting Information], (b) intermediate frequency modes, and (c) G-band dispersion.

0.55 nm are identified (Figure 3a). This diameter shift correlates very well with the variation in catalyst particle size determined by EXAFS. High-resolution TEM images were collected for SWNT bundles synthesized at the lowest temperature (Figure 3d). Multiple images collected at different points on the sample showed a vast majority of the SWNTs to have diameters <1 nm. Most imaged tubes appear to have diameters around 0.6 nm, which correlates well with the values from the Raman data.

Kataura et al.[25] proposed the use of a simple plot between the electronic transition energy (E_{ii}) and d_t for analyzing various optical properties of SWNTs. Specifically, resonant Raman spectra of large-diameter SWNTs ($d_t > 1$ nm) can be used along with the Kataura plot for (*n*,*m*) assignment. Following Kataura, Weismann et al.[19] developed an empirical plot of E_{ii} vs d for better (*n*,*m*) assignment in a wider diameter range (~0.5−2 nm). However, it is important to note that consideration of other optical absorption data along with the Raman spectra to eliminate any possible ambiguity in the assigned chirality (*n*,*m*) indexing based solely on absorption data[26,27] (or Raman spectra) may not be appropriate for several reasons: (i) Techniques such as PL can only probe semiconducting nanotubes, and the quantification of (*n*,*m*) species becomes complicated, as the intensity of the emission strongly depends on how far the absorption energy is from the excitation energy.[27] (ii) It presumes the same extinction coefficients for every possible (*n*,*m*). (iii) Most importantly, since E_{ii} strongly depends on $1/d$, one generally observes broad (poorly resolved) peaks in the optical absorption, and thus the (*n*,*m*) identification is more difficult.[28] Hence, we used Raman in tandem with PL to assign the chirality in sub-nm SWNTs (Table 2 and Supporting Information Figure S3a−c). Such indexing is possible in the case of sub-nm SWNTs ($\omega_{RBM} > 240$ cm^{-1}), as the number of chiralities that can be resonant in the excitation window of $488 < \lambda_{excitation} < 1064$ nm is limited.[25] The set of wavelengths (488−1064 nm) used for characterizing our samples can excite both semiconducting tubes with diameters between 0.5 and 1.75 nm and metallic tubes with diameters between 0.6 and 2 nm. Using Raman and PL spectra in tandem, the (*n*,*m*) indices were identified as follows: (i) d_t

Table 2. (*n*,*m*) Chiralities Identified by Raman and PL Spectroscopy in the SWNT Samples Synthesized at Various Temperatures on the CoMn-MCM-41 Catalyst

tube	diameter, nm	metallic or semiconducting	CoMn, 600 °C		CoMn, 700 °C		CoMn, 800 °C	
			Raman	PLE	Raman	PLE	Raman	PLE
(4,3)	0.48	S	Y	N	N	N	N	N
(5,3)	0.55	S	Y	N	N	N	N	N
(5,4)	0.62	S	Y	N	Y	N	N	N
(5,5)	0.68	M	Y	N	N	N	N	N
(6,4)	0.69	S	Y	N	N	N	N	N
(6,5)	0.75	S	Y	Y	Y	Y	Y	Y
(7,0)	0.55	S	Y	N	Y	N	N	N
(7,1)	0.59	M	N	N	N	N	Y	N
(7,3)	0.70	S	Y	Y	Y	Y	Y	N
(7,4)	0.76	M	N	N	Y	N	Y	N
(7,5)	0.82	S	Y	Y	Y	Y	Y	Y
(7,6)	0.89	S	Y	Y	Y	Y	Y	Y
(8,1)	0.68	S	Y	N	Y	N	N	N
(8,3)	0.78	S	Y	Y	Y	Y	Y	Y
(8,4)	0.84	S	N	N	Y	Y	Y	Y
(8,6)	0.96	S	Y	Y	Y	Y	Y	Y
(8,7)	1.03	S	N	N	N	Y	Y	Y
(9,2)	0.80	S	Y	Y	N	Y	N	N
(9,4)	0.91	S	N	N	Y	Y	N	Y
(9,5)	0.97	S	Y	N	Y	Y	Y	Y
(9,6)	1.03	M	N	N	Y	N	N	N
(9,7)	1.10	S	Y	Y	Y	Y	Y	Y
(9,8)	1.17	S	N	N	Y	N	N	N
(10,1)	0.83	M	N	N	Y	N	N	N
(10,3)	0.93	S	N	N	N	N	Y	Y
(10,7)	1.17	M	N	N	N	N	Y	N
(10,9)	1.30	S	N	N	N	N	Y	N
(10,10)	1.37	M	N	N	N	N	Y	N
(11,2)	0.96	M	N	N	Y	N	N	N
(11,3)	1.01	S	N	N	N	N	Y	N
(11,8)	1.31	M	N	N	N	N	Y	N
(12,6)	1.26	M	N	N	N	N	Y	N
(12,9)	1.45	M	N	N	N	N	Y	N
(14,2)	1.19	M	N	N	N	N	Y	N
(18,2)	1.51	S	N	N	N	N	Y	N

(25) Kataura, H.; Kumazawa, Y.; Maniwa, Y.; Umezu, I.; Suzuki, S.; Ohtsuka, Y.; Achiba, Y. *Synth. Met.* **1999**, *103*, 2555.
(26) Li, X.; Tu, X.; Zaric, S.; Welsher, K.; Seo, W. S.; Zhao, W.; Dai, H. *J. Am. Chem. Soc.* **2007**, *129*, 15770.
(27) Lolli, G.; Zhang, L.; Balzano, L.; Sakulchaicharoen, N.; Tan, Y.; Resasco, D. E. *J. Phys. Chem. B* **2006**, *110*, 2108.
(28) Nikolaev, P.; Holmes, W.; Sosa, E.; Boul, P.; Arepalli, S.; Yowell, L. *J. Nanosci. Nanotech.* **2010**, *10*, 3780.

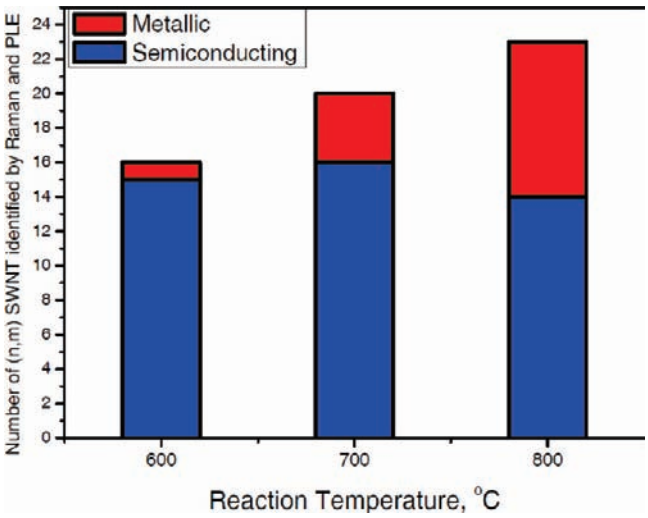

Figure 6. Number of metallic and semiconducting sub-nm SWNTs found in samples shown in Figure 1a as determined by (*n*,*m*) indices obtained from PL and Raman spectroscopy.

was estimated from the observed ω_{RBM} using eq 1, and the chiral angles were computed from the E_{ii} values obtained through the best-fit equation (eq 2b in ref 19) to the empirical Kataura plot described in ref 25. (ii) A chiral vector, obtained from a given d_t and its chiral angle from the previous step, was then used along with PL spectra to uniquely identify the (*n*,*m*) index (Table 2).

We conclude that low synthesis temperature (~600 °C) favors (~ 93%) the growth of semiconducting sub-nm SWNTs (Figure 6). We attribute this dependence on the synthesis temperature to the size and shape of Co particles in the presence of Mn, which presumably leads to the formation of graphitic caps for semiconducting sub-nm SWNTs. These results are important since they demonstrate a simple, scalable method for direct production of sub-nm SWNT populations highly enriched in semiconducting SWNTs.

The preferential growth of semiconducting SWNTs at the lower reaction temperature was further analyzed from the catalyst standpoint. As mentioned before, we attribute this effect to the change in size and shape of the catalyst particles with reaction temperature. First it was demonstrated by EXAFS that the catalytic particles in the sample synthesized at 600 °C were, on average, 0.45 nm smaller than those in the sample reacted at 800 °C. As expected, this leads to a similar variation in the average tube diameter (smaller average diameter at the lower temperature), as evident from the Raman and PL data. Li and co-workers[29] have conducted density functional theory calculations to investigate the energetics and stability of various types of nanotubes. They have studied the variation of the heat of formation with diameter for semiconducting and metallic SWNTs and found that, for sub-nm SWNTs, the energy cost for extending the tube length by a C−C bond is higher for a metallic nanotube than for a semiconducting one. This difference becomes more significant as the average tube diameter decreases. Their calculations are consistent with the experimental results presented here.

Catalyst particle shape is also likely a contributing factor.[30,31] Even though the catalytic particles are not readily accessible to microscopy investigations since they are embedded in the silica pore wall, variations in the shape can be probed by magnetic measurements. A superconducting quantum interference device (SQUID) measurement carried out at 40 K for the as-reacted samples at 600 and 800 °C revealed some interesting differences (see Figure S3 in the Supporting Information). The two samples were chosen because they showed the highest and the lowest semiconducting SWNT proportion, respectively. The SQUID data were used to determine the coercivity (the intensity of the applied magnetic field required to reduce the magnetization of that material to zero *after* the magnetization of the sample has been driven to saturation). For soft magnetic materials such as Co nanoparticles, the intrinsic magneto crystalline anisotropy is expected not to contribute significantly to the total anisotropy. As a consequence, shape anisotropy is predicted to produce the largest coercive forces,[32] and thus coercivity for very small particles is a good measure of deviation from spherical shape. For superparamagnetic, single-domain Co particles, coercivity is not expected to be affected by changes in the particle size at diameters <35 nm.[33] In our case, therefore, we can safely remove particle size variability as a factor affecting the coercivity. The measured values from the data presented in Figure S3 were 53 Oe for the sample reacted at 600 °C and 14 Oe for the sample reacted at 800 °C. On the basis of these measurements, we conclude that the particles formed at the lowest reaction temperature have the highest shape anisotropy (deviation from spherical shape). A difference in shape of the nucleating particles can affect the formation of the carbon cap by inducing variation of the surface free energy, making the formation of particular carbon caps more likely.[30] Reich and co-workers have used *ab initio* calculations to show that particular caps could be favored by their epitaxial relationship to the solid catalyst surface and that the lattice-matched caps and tubes are more stable than non-lattice-matched structures.[31]

The difference in shape and size between the particles formed at the different reaction temperatures is very likely responsible for the preferential formation of such a high proportion of sub-nm semiconducting SWNTs.

Further evidence of the semiconducting nature of the sample is offered by the shape of the G-band feature (Figures 3c, 4c, and 5c). The G-band feature of a SWNT has two components. The higher frequency component (G+) around 1600 cm^{-1} is associated with vibrations along the nanotube axis, while the lower frequency component (G−) around 1560 cm^{-1} is attributed to vibrations in the circumference of the tube. For metallic nanotubes, the lower frequency peak is a broad Breit−Wigner−Fano (BWF) line shape rather than a Lorentzian shape as is the case for semiconducting nanotubes.[34−37] If we assume our SWNT samples to be a mixture of semiconducting and metallic tubes, examination of the G− region should prove useful in bringing further evidence to support our previous conclusions. For the sample synthesized at 800 °C, the G− component shows a broad, asymmetric shape around 1560 cm^{-1}, which is characteristic for a mixture of semiconducting and metallic tubes. This feature is partially suppressed for the sample

(29) Li, Y.; Peng, S.; Mann, D.; Cao, J.; Tu, R.; Cho, K.; Dai, H. *J. Phys. Chem. B* **2005**, *109*, 6968.
(30) Harutyunyan, A.; Chen, G.; Paronyan, T.; Pigos, E.; Kuznetsov, O.; Hewaparakrama, K.; Kim, S.; Zakharov, D.; Stcah, E.; Sumanasekera, G. *Science* **2009**, *326*, 116.
(31) Reich, S.; Li, l.; Robertson, J. *Chem. Phys. Lett.* **2006**, *421*, 469.
(32) Li, H.; Chen, C. *Phys. Rev. B* **2007**, *75*, 184424-1.
(33) Leslie-Pelecky, D. *Chem. Mater.* **1996**, *8*, 1770.

reacted at 700 °C, suggesting that the proportion of excited metallic tubes is decreased. At 600 °C, the BWF feature is completely suppressed in the spectra collected at the various wavelengths, indicating a large increase in the proportion of semiconducting tubes within individuals resonating with our seven excitation energies.

Interestingly, we observed "S"-shaped dispersion of the G-band frequency as a function of the laser excitation energy (see Figures 3c, 4c, and 5c and Supporting Information Figure S2a−c). It should be noted that, in past studies of SWNTs with diameters >1 nm, the G-band frequency was not observed to be affected by curvature.[38] The G-band is observed to soften (downshift) at first ($488 < \lambda_{excitation} < 514.5$ nm) and then harden (upshift) with increasing excitation wavelength ($532 < \lambda_{excitation} < 785$ nm), which is then followed by re-softening of the optical phonon ($785 < \lambda_{excitation} < 1064$ nm) in an "S"-shape. We relate this dispersion of G-band to electron−phonon interaction and perturbation of optical phonon energy due to high curvature in sub-nm SWNTs. Independent studies on the mechanism behind such dispersion will be published later.

To measure electric transport, powder samples of the sub-nm SWNTs synthesized at 600, 700, and 800 °C were purified by a procedure that included refluxing with a NaOH solution to remove the silica matrix and treatment with HCl to remove the metal particles. The purified SWNTs were then loaded and pressed into pellets of 5 mm diameter with 1 psi of pressure by a manual hydraulic press for about 2 min. Electrical contact was made to the top and bottom of each pellet using high-purity conductive silver paint. The resistance through the SWNT pellet was measured in a two-probe configuration at temperatures ranging from 275 to 4.2 K. The two-terminal resistances of the 600, 700, and 800 °C SWNT pellets at $T = 275$ K were approximately 20 Ω, 2 Ω, and 8 Ω, respectively. The resistances of the 600, 700, and 800 °C SWNT pellets at $T = 4.2$ K were approximately 10 kΩ, 1 kΩ, and 600 Ω, respectively. The normalized dc resistance as a function of temperature for all three pellets is presented in Figure 7. A nonmetallic temperature dependence of the resistance is displayed for all three pellets and is attributed to hopping conduction between weakly coupled nanotubes.[39] The SWNT pellet synthesized at 600 °C demonstrates the greatest normalized resistance increase with decreasing temperature, consistent with a higher percentage of semiconducting SWNTs. The SWNT pellet synthesized at 800 °C exhibited the smallest normalized resistance increase with decreasing temperature, consistent with a lower percentage of semiconducting SWNTs. These electrical transport measurements agree with the conclusion that low synthesis temperature favors the growth of semiconducting sub-nm SWNTs.

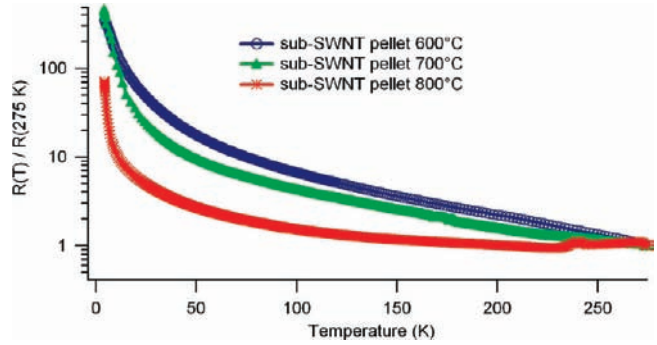

Figure 7. Normalized resistance on a log scale as a function of temperature for three different pellets of sub-nm SWNTs synthesized at 600, 700, and 800 °C. The observed behavior suggests that the low synthesis temperature (600 °C) favors growth of semiconducting sub-nm SWNTs as compared to the higher synthesis temperatures.

3. Conclusion

A simple and scalable approach for the direct production of diameter-selective semiconducting sub-nm SWNTs was demonstrated using a CoMn-MCM-41 bimetallic catalyst. Raman and PL spectra were used in tandem for identifying (*n*,*m*) indices of these sub-nm SWNTs. In addition, the effect of synthesis temperature on diameter and (*n*,*m*) index of sub-SWNTs was also explained. New features observed in the Raman spectra of sub-nm SWNTs (IFM and S-shaped dispersion of G-band) were presented.

Acknowledgment. We gratefully acknowledge financial support from NSF D01521 834 and MURI L00096. We thank the NSLS beam lines X18B and X23A2 at Brookhaven National Laboratory for use of their facilities and acknowledge Profs. Nebojsa Marinkovic and Bruce Ravel for their support in collecting the EXAFS data.

Supporting Information Available: Fitting results of the EXAFS data, abundance of main tubes identified by PLE, Raman spectra collected at different wavelengths, (*n*,*m*) indexing of the RBM region of the Raman spectra, and SQUID measurements of the as-reacted catalysts. This material is available free of charge via the Internet at http://pubs.acs.org.

JA102011H

(34) Yu, Z.; Brus, L. *J. Phys. Chem. B* **2001**, *105*, 1123.
(35) Harutyunyan, A.; Chen, G.; Parnoyan, T.; Pigos, E. M.; Kuznetsov, O. A.; Hewaparakrama, K.; Kim, S. M.; Zakharov, D.; Stach, E.; Sumanasekera, G. V. *Science* **2009**, *326*, 116.
(36) Pimenta, M. A.; Marucci, A.; Empedocles, S. A.; Bawendi, M. G.; Hanlon, E. B.; Rao, A. M.; Eklund, P. C.; Smalley, R. E.; Dresselhaus, G.; Dresselahus, M. S. *Phys. Rev. B* **1998**, *58*, 16016.
(37) Yin, Y.; Walsh, A. G.; Vamivakas, A. N.; Cronin, S. B.; Stolyarov, A. M.; Timkhan, M.; Bacsa, W.; Unlu, M. S.; Goldberg, B. B.; Swan, A. K. *IEEE J. Sel. Top. Quantum Electron.* **2006**, *12*, 1083.
(38) Rao, A. M.; Richter, E.; Bandow, S.; Chase, B.; Eklund, P. C.; Williams, K. A.; Fang, S.; Subbuswamy, K. R.; Menon, M.; Thess, A.; Smalley, R. E.; Dresselhaus, G.; Dresselahus, M. S. *Science* **1997**, *275*, 187.
(39) Chauvet, O.; Benoit, J. M.; Corraze, B. *Carbon* **2004**, *42*, 949.